JPET Fast Forward. Published on July 20, 2017 as DOI: 10.1124/jpet.117.242990
This article has not been copyedited and formatted. The final version may differ from this version.

Mechanistic Multi-Tissue Modeling of GILZ Regulation: Integrating Circadian Gene Expression with Receptor-Mediated Corticosteroid Pharmacodynamics

Vivaswath S. Ayyar, Debra C. DuBois, Richard R. Almon, William J. Jusko

Department of Pharmaceutical Sciences, School of Pharmacy and Pharmaceutical Sciences, State University of New York at Buffalo, Buffalo, NY, 14214 (V.S.A., D.C.D, R.R.A, W.J.J.); Department of Biological Sciences, State University of New York at Buffalo, Buffalo, NY, 14260 (D.C.D, R.R.A)

JPET Fast Forward. Published on July 20, 2017 as DOI: 10.1124/jpet.117.242990
This article has not been copyedited and formatted. The final version may differ from this version.

Running Title: Modeling Tissue-Specific Pharmacogenomics of Steroid Action

Corresponding author:

William J. Jusko, Ph.D.

Department of Pharmaceutical Sciences

School of Pharmacy and Pharmaceutical Sciences

State University of New York at Buffalo

Buffalo, NY, 14214

E-mail: wjjusko@buffalo.edu

Telephone: 716-645-2855

Fax: 716-829-6569

Number of text pages: 25

Number of tables: 3

Number of figures: 10

Number of references: 59

Number of words:

Abstract: 249

Introduction: 711

Discussion: 1500

List of non-standard abbreviations: adrenalectomized, ADX; CS, corticosteroid; CST, corticosterone; GILZ, glucocorticoid-induced leucine zipper; GR, glucocorticoid receptor; GRE, glucocorticoid-response element; IDR, indirect response; MPL, methylprednisolone; PK/PD/PG, pharmacokinetic, pharmacodynamic and pharmacogenomic; qRT-PCR, quantitative real-time reverse transcription-polymerase chain reaction

Recommended Section: Other

ABSTRACT

The glucocorticoid-induced leucine zipper (GILZ) is an important mediator of anti-inflammatory corticosteroid action. The pharmacokinetic/pharmacodynamic/pharmacogenomic effects of acute and chronic methylprednisolone (MPL) dosing on the tissue-specific dynamics of GILZ expression were examined in rats. A mechanism-based model was developed to investigate and integrate the role of MPL and circadian rhythms on the transcriptional enhancement of GILZ in multiple tissues. Animals received a single 50 mg/kg intramuscular bolus or a seven-day 0.3 mg/kg/h subcutaneous infusion of MPL and were euthanized at several time-points. An additional group of rats were euthanized at several times and served as 24-h light/dark (circadian) controls. Plasma MPL and corticosterone concentrations were measured by high-performance liquid chromatography. The expression of GILZ and glucocorticoid receptor (GR) mRNA was quantified in tissues using qRT-PCR. The pharmacokinetics of MPL were described using a two-compartment model. Mild-to-robust circadian oscillations in GR and GILZ mRNA expression were characterized in muscle, lung, and adipose tissues and modeled using Fourier harmonic functions. Acute MPL dosing caused significant down-regulation (40-80%) in GR mRNA and enhancement of GILZ mRNA expression (500-1080%) in the tissues examined. While GILZ returned to its rhythmic baseline following acute dosing, a new steady-state was observed upon enhancement by chronic dosing. The model captured the complex dynamics in all tissues for both dosing regimens. The model quantitatively integrates physiological mechanisms such as circadian processes and GR tolerance phenomena, which control the tissue-specific regulation of GILZ by corticosteroids. These studies characterize GILZ as a pharmacodynamic marker of corticosteroid actions in several tissues.

Introduction

Corticosteroids (CS) are potent anti-inflammatory and immunosuppressive drugs widely used in treating diseases such as rheumatoid arthritis (RA) (Kirwan, 1995), asthma (Barnes, 1998), and some lymphomas (Kofman et al., 1962). They exert both therapeutic and adverse effects in tissues upon binding the ubiquitously expressed glucocorticoid receptors (GR). Upon binding the GR, CS can cause effects which are rapid in onset such as cell trafficking and adrenal suppression (Yao et al., 2008). In contrast, pharmacogenomic regulation by the drug-receptor complex occurs in a delayed fashion (Jusko, 1995), due to a series of intracellular transduction steps, including gene regulation and consequent mRNA and protein synthesis. In this manner, CS dosing elicits widespread changes in gene expression in multiple tissues (Almon et al., 2005a; Almon et al., 2005b; Almon et al., 2007b).

One such gene that is highly regulated by CS is the glucocorticoid-induced leucine zipper (GILZ). GILZ has emerged as an important mediator of the anti-inflammatory actions of CS (Ayroldi and Riccardi, 2009). Its major mechanism of action involves binding to the p65-subunit of NFκB (Di Marco et al., 2007) and thereby repressing its translocation into the nucleus, and consequent pro-inflammatory gene expression. Recent evidence also demonstrates its role in modulating tumor growth and cell proliferation (Ayroldi et al., 2015; Bruscoli et al., 2015). Therefore, pharmacologic enhancement of GILZ will influence CS therapy.

Many CS-regulated genes, including GILZ, have been previously examined. However, most studies were performed *in vitro*, and hence, are unable to provide holistic information regarding underlying systemic and tissue-specific processes. Furthermore, little is known regarding the temporal patterns of CS-regulated genes *in vivo* and their governing mechanisms. Development of mechanistic pharmacokinetic and pharmacodynamic (PK/PD) models is essential for gaining quantitative understanding of the physiological and pharmacological mechanisms underlying the time-course of diverse drug responses. Such PK/PD models have been developed in our laboratory to describe the receptor/gene-mediated effects of steroids on target genes such as tyrosine aminotransferase (TAT) (Ramakrishnan et al., 2002a), glutamine synthetase

(GS) (Sun et al., 1999), and phosphoenolpyruvate carboxylase (PEPCK) (Jin et al., 2004) in adrenalectomized (ADX) rats.

Although TAT, GS, and PEPCK are useful biomarkers to probe the genomic effects of CS, they share a common limitation – in vivo expression is confined to one or two tissues. The rate-limiting enzyme in tyrosine metabolism, TAT, lacks a direct clinical relevance. PEPCK, which catalyzes the rate-limiting step of gluconeogenesis, is regulated by various hormones including CS, glucagon, and insulin; confounding the simple assessment of CS effects alone. In contrast, several features make GILZ a robust marker to investigate CS sensitivity. First, GILZ is ubiquitously expressed in multiple tissues in man and in the rat (Cannarile et al., 2001; Ayyar et al., 2015). Second, GILZ shows exquisite sensitivity to enhancement by CS due to the presence of multiple functional GREs in its 5'-upstream promoter region (van der Laan et al., 2008). Finally, GILZ expression is, at least in part, directly related to the anti-inflammatory efficacy of CS.

Since adrenal release of endogenous glucocorticoid hormones occurs in a rhythmic manner, their downstream target genes in peripheral tissues may be expected to follow similar oscillations. Indeed, many steroid-regulated genes, including cholesterol-7a-hydroxylase, TAT, and GR exhibit circadian rhythms (Van Cantfort and Gielen, 1979; Sukumaran et al., 2010). GILZ also demonstrates a circadian rhythm *in vivo*, which is entrained to that of plasma corticosterone (CST) in rats (Ayyar et al., 2015). Such circadian responses add time-dependent complexities (Jusko, 1995), which must be accounted for while evaluating drug effects.

We developed and applied a mechanism-based PK/PD/pharmacogenomic (PK/PD/PG) model with circadian-controlled processes that describe the tissue-specific dynamics of GILZ mRNA expression in skeletal muscle, lung, and white adipose tissue. The GILZ and GR mRNA dynamics were examined in intact (non-ADX) rats to evaluate concerted effects of circadian rhythms and CS pharmacodynamics. The mechanistic model was fitted simultaneously to data from untreated and single-dosed animals to yield tissue-specific information on drug- and system-specific parameters. Simulations were performed to predict the GILZ mRNA dynamics in lung and adipose tissue upon chronic dosing and gain new insights into the

tissue- and dose regimen-dependent aspects controlling receptor-mediated gene expression *in vivo*. Collectively, these studies provide a quantitative and mechanistic framework for the application of GILZ as a PD marker of a CS anti-inflammatory mediator in tissues of clinical relevance.

Materials and Methods

Animals

Experiments utilized tissue samples harvested from three separate population-based animal studies conducted in our laboratory. An extensive description of these studies can be found in previously published reports (Hazra et al., 2007a; Almon et al., 2008; Ayyar et al., 2015). Brief descriptions of the studies are provided here. In all studies, normal male Wistar rats were acclimated and housed under a 12 h:12 h light:dark cycle and constant-temperature (22°C) environment, with free access to drinking water and standard rat chow. All animals were housed in separate cages to facilitate animal manipulations while minimizing stress to the animals. The rats were euthanized by aortic exsanguination under ketamine/xylazine anesthesia (80:10 mg/kg). Blood samples were harvested using EDTA as an anticoagulant. Plasma was prepared from blood by centrifugation (2000g, 4°C, 15 min), aliquoted, and stored at −80°C until further analyses. Several tissues including abdominal adipose, lung and skeletal muscle were rapidly excised, flash frozen in liquid nitrogen, and stored at -80°C. Animals euthanized at the same time point were treated as triplicate measurements in each study. All animal study protocols adhered to the "Guide for the Care and Use of Laboratory Animals, 8th Edition" (National research Council, 2011) and were approved by the State University of New York at Buffalo Institutional Animal Care and Use Committee.

Experimental

Circadian study. Fifty-four normal male Wistar rats purchased from Harlan Laboratories (Indianapolis, IN, USA) were housed and allowed to acclimatize in a room equipped with a 12-h light/dark cycle, and were subject to minimal environmental disturbance. Animals were euthanized by exsanguination on three successive days at 18 different time-points ranging from 15 minutes to 23.75 hours after lights went on (n = 3 animals per time point).

Single MPL bolus study. Sixty normal male Wistar rats purchased from Harlan Laboratories were utilized. Each animal was given a single 50 mg/kg intramuscular (IM) bolus dose of methylprednisolone sodium succinate (Solu-Medrol, Upjohn, Kalamazoo, MI) in the left hind haunch between 1.5 and 3 hours after lights on (i.e. at the nadir of the circadian pattern of the endogenous CST rhythm). Animals were euthanized at 18 different time-points ranging from 15 minutes to four days (96 hours) after receiving MPL injection (n = 3 animals per time point). Control animals were euthanized in triplicate at 12 and 24 hours after saline injection.

Chronic MPL infusion study. Thirty-nine normal male Wistar rats were purchased from Harlan-Sprague Dawley Inc. (Indianapolis, IN). The treatment group (n = 27) were given 0.3 mg/kg/h of methylprednisolone sodium succinate (Solu-Medrol) via subcutaneously (SC) implanted Alzet osmotic mini-pumps (Model 2001, Alza, Palo Alto, CA). Animals in the control group (n = 12) were implanted with vehicle-filled pumps. MPL-dosed animals were euthanized over seven days following pump implantation (n = 3 animals per time point). Vehicle controls were euthanized at 6, 12, 18 and 24 hours post pump implantation (n = 3 animals per time point).

Drug and Endogenous Steroid Assay

Plasma CST and MPL concentrations were determined by a normal-phase high-performance liquid chromatography method (Haughey and Jusko, 1988). The limit of quantitation was 5 ng/mL for CST and 10 ng/mL for MPL. The inter-day and intra-day coefficients of variation (CV) were less than 10%.

RNA Preparation

Frozen tissue samples were ground into a fine powder under liquid nitrogen. Powdered samples were weighed, added to pre-chilled TRI Reagent (Invitrogen, Carlsbad CA), and homogenized. Total RNA extractions were carried out using TRI Reagent and further purified by passage through RNeasy mini-columns (QIAGEN, Valencia, CA) according to manufacturer's protocols for RNA clean-up. The RNA concentrations were quantified spectrophotometrically (NanoDrop 2000c, Thermo Scientific, MA), and

purity and integrity were assessed by agarose-formaldehyde gel electrophoresis. All samples exhibited 260/280 absorbance ratios of approximately 2.0, and all showed intact ribosomal 28S and 18S RNA bands in an approximate ratio of 2:1 as visualized by ethidium bromide staining. Final total RNA preparations were diluted to desired concentrations in nuclease-free water (Ambion, Austin, TX, USA) and stored in nuclease-free tubes at −80°C until use.

Quantification of mRNA Expression

The GILZ- and GR-specific quantitative real-time polymerase chain reaction (qRT-PCR) assays were developed and validated according to the Minimum Information for Publication of Quantitative Real-Time PCR Experiments (MIQE) guidelines (Bustin et al., 2009). Both qRT-PCR assays involved use of *in vitro* transcribed cRNA standards, gene-specific TaqMan-based probes, and a single-step assay. An extensive description on the sub-cloning and construction of the *in vitro* transcribed cRNA standards was reported previously (Ayyar et al., 2015). Primer and probe sequences were designed and custom-synthesized (Biosearch Technologies, Novato, CA). qRT-PCR was performed using a Brilliant qRT-PCR Core Reagent Kit, 1-Step (Stratagene, La Jolla, CA) in a Stratagene MX3005P thermocycler according to the manufacturer's instructions. Primer and probe sequences were as follows: GR, forward primer 5′-AACATGTTAGGTGGGCGTCAA-3′, reverse primer 5′-GGTGTAAGTTTCTCAAGCCT AGTATCG-3′ and FAM-labeled probe, 5′-TGATTGCAGCAGTGAAATGGGCAAAG-3′; GILZ, forward primer 5’-GGAGGTCCTAAAGGAGCAGATTC- 3’, reverse primer 5’- GCGTCTTCAGGAGGG TATTCTC- 3’ and FAM-labeled probe, 5’-TGAGCTGGTTGAGAAGAACTCGCA- 3’. Standards were run in duplicate and samples in triplicate; intra- and inter-assay CV were less than 20%. Additional reverse-transcriptase minus controls were included to ensure lack of DNA contamination in each sample.

Pharmacokinetic/Pharmacodynamic/Pharmacogenomic Modeling

Pharmacokinetics.

JPET Fast Forward. Published on July 20, 2017 as DOI: 10.1124/jpet.117.242990
This article has not been copyedited and formatted. The final version may differ from this version.

A two-compartment model with dual absorption pathways from the injection site was used to describe the PK of IM dosing of MPL (Hazra et al., 2007b). The PK parameters were fixed with estimates obtained from our previous study as given in Table 1. Equations and initial conditions (IC) describing the model are:

$$V_C \frac{dC_p}{dt} = k_{a1} \cdot D_{(IM)} \cdot F \cdot F_r \cdot e^{-k_{a1}t} + k_{a2} \cdot D_{(IM)} \cdot F \cdot (1 - F_r) \cdot e^{-k_{a2}t} - CL \cdot C_P - CL_D \cdot C_P + CL_D \cdot C_T \qquad IC = 0 \quad (1)$$

$$V_T \frac{dC_T}{dt} = CL_D \cdot C_P - CL_D \cdot C_T \qquad IC = 0 \quad (2)$$

where *C* and *D* represent the concentration and dose of MPL in the corresponding plasma (*P*) and tissue (*T*) compartments, F_r and $(1 - F_r)$ are fractions of dose absorbed through the absorption pathways described by first-order rate constants k_{a1} and k_{a2}, *CL* is clearance from the central compartment, CL_D is the distribution clearance, *F* is the overall bioavailability of MPL after IM injection, and V_c and V_T are the central and peripheral volumes of distribution.

The same equations were employed for the SC infusion kinetics, with the exception that a zero-order input function (0.3 mg/kg/h) was applied instead of the two first-order absorption terms. Distribution-related parameters (V_c, V_T, and CL_D) were fixed based on the bolus data, whereas the clearance (*CL*) was estimated from the infusion data as shown in Table 1. The pharmacokinetic model schematic for both dosing regimens is depicted in Figure 1. Plasma drug concentrations over time were fixed and used as a driving force for the dynamics in the subsequent data analysis.

Mechanistic Basis for Pharmacodynamics

The diverse cellular and molecular processes that govern the pharmacodynamic and pharmacogenomic effects of CS are depicted in Figure 2. Approximately 77% of circulating CS in plasma is bound to corticosteroid-binding globulin (CBG) and albumin (Haughey and Jusko, 1992). Owing to its moderate lipophilicity, free (unbound) CS can passively diffuse across cell membranes into the cytosol, where GR is located. Inactive GR is held and stabilized in the cytoplasm by molecular chaperones including heat shock proteins (hsp 70 and 90) as well as the FK506-binding protein (FKBP) immunophilins (Pratt

and Toft, 1997). The CS bind to cytoplasmic GR and cause a dissociation of the chaperone complex by inducing a conformational change in the GR molecule. Upon dissociation from chaperone proteins, activated drug-receptor complexes rapidly translocate into the nucleus and homodimerize. The complexes then bind specific DNA sequences known as GREs in the 5'-upstream promoter regions of target genes, leading to transcriptional changes by altering chromatin structure (Newton, 2000; Barnes, 2006) and consequent activation of the RNA-polymerase complex. This genome-level interaction positively or negatively regulates the expression of a plethora of genes. *De novo* synthesized RNA transcripts undergo 5'-capping, splicing, and 3'-polyadenylation to form mRNA, which are exported to the cytoplasm. mRNA transcripts, in this case those encoding GILZ, are then translated into protein and/or degraded within the cytoplasm – leading to alterations in measurable mRNA and protein concentrations.

After exerting their transcriptional effects, the steroid-receptor complexes in the nucleus may dissociate from GREs, and return to the cytosol. Part of the receptors may be degraded during the process, whereas the rest may be reassembled with chaperone proteins and recycled. Therefore, the total pool of free cytosolic GR constitutes a composite of recycled and *de novo* synthesized GR molecules. Furthermore, the CS cause homologous down-regulation of their own receptors via decreased transcription, which subsequently results in decreased mRNA synthesis and free GR densities in the cytosol (Oakley and Cidlowski, 1993; DuBois et al., 1995).

Mathematical Model

Figure 3 depicts the integrated PK/PD/PG model that describes the tissue-specific effects of CS and circadian oscillations on the regulation of GILZ gene expression.

Glucocorticoid Receptor Dynamics

The dynamics of GR have been previously studied in liver and adipose tissue from normal male rats (Hazra et al., 2008; Sukumaran et al., 2011). Kinetic parameter values governing drug-receptor binding, translocation, and recycling were fixed to previously obtained values (Hazra et al., 2007a) since these

JPET Fast Forward. Published on July 20, 2017 as DOI: 10.1124/jpet.117.242990
This article has not been copyedited and formatted. The final version may differ from this version.

processes are considered to be similar across different tissues. The differential equations and initial conditions for GR dynamics in the tissues are:

$$\frac{dR}{dt} = k_{s,GR} \cdot GR_m - k_{d,GR} \cdot R - k_{on} \cdot f_{mpl} \cdot C_{mpl} \cdot R + k_{re} \cdot R_f \cdot DR_n \qquad IC = R(0) \quad (3)$$

$$\frac{dDR}{dt} = k_{on} \cdot f_{mpl} \cdot C_{mpl} \cdot R - k_t \cdot DR \qquad IC = DR(0) \quad (4)$$

$$\frac{dDR_n}{dt} = k_t \cdot DR - k_{re} \cdot DR_n \qquad IC = DR_n(0) \quad (5)$$

where symbols are the free cytosolic receptor (*R*), cytosolic drug-receptor complex (*DR*), and nuclear translocated drug-receptor complex concentrations (DR_n). The rate constants include receptor synthesis ($k_{s,GR}$) and degradation ($k_{d,GR}$), translocation of the drug-receptor complex into the nucleus (k_T), the overall turnover of DR_n return receptors to cytosol (k_{re}), as well as the second-order rate constant of drug-receptor association (k_{on}). Part of DR_n may recycle back to the cytosol controlled by the rate constant $R_f \cdot k_{re}$ and the rest gets degraded with a rate constant $(1-R_f) \cdot k_{re}$. The f_{mpl} is the unbound fraction of MPL in plasma.

The GR mRNA (GR_m) showed circadian oscillations in muscle, lung, and adipose, which were described using an indirect response (IDR) model with the mRNA synthesized by a time-dependent synthesis rate ($k_{s,GRm(t)}$) and degraded by first-order rate constant ($k_{d,GRm}$) as follows:

$$\frac{dGR_m}{dt} = k_{s,GRm}(t) - k_{d,GRm} \cdot GR_m \qquad IC = GR_m(0) \quad (6)$$

The time-dependent synthesis rate of GR mRNA [$k_{s,GRm(t)}$] in adipose tissue was described using a two harmonic function as reported previously (Sukumaran et al., 2011), whereas single harmonic functions were applied for the same in skeletal muscle and lung:

$$k_{s,GRm,adipose}(t) = a_{0,GRm} \cdot k_{d,GRm} + \left(a_{1,GRm} \cdot k_{d,GRm} + \frac{2\pi b_{1,GRm}}{24}\right) \cdot cos\left(\frac{2\pi T}{24}\right)$$
$$+ \left(b_{1,GRm} \cdot k_{d,GRm} + \frac{2\pi a_{1,GRm}}{24}\right) \cdot sin\left(\frac{2\pi T}{24}\right) + \left(a_{2,GRm} \cdot k_{d,GRm} + \frac{2\pi b_{2,GRm}}{12}\right) \cdot cos\left(\frac{2\pi T}{12}\right)$$
$$+ \left(b_{2,GRm} \cdot k_{d,GRm} + \frac{2\pi a_{2,GRm}}{12}\right) \cdot sin\left(\frac{2\pi T}{12}\right) \quad (7)$$

JPET Fast Forward. Published on July 20, 2017 as DOI: 10.1124/jpet.117.242990
This article has not been copyedited and formatted. The final version may differ from this version.

$$k_{s,GRm,lung/muscle}(t) = a_{0,GRm} \cdot k_{d,GRm} + \left(a_{1,GRm} \cdot k_{d,GRm} + \frac{2\pi b_{1,GRm}}{24}\right) \cdot$$

$$cos\left(\frac{2\pi T}{24}\right) + \left(b_{1,GRm} \cdot k_{d,GRm} + \frac{2\pi a_{1,GRm}}{24}\right) \cdot sin\left(\frac{2\pi T}{24}\right) \quad (8)$$

where a_i and b_i are Fourier coefficients associated with the harmonic oscillations. Values for these parameters were obtained by fitting the replicate GR mRNA expression data measured in each tissue from the circadian control study using the FOURPHARM program (Krzyzanski et al., 2000).

Suppression in GR mRNA expression by MPL is given by:

$$\frac{dGR_{m,mpl}}{dt} = k_{s,GRm(t)} \cdot \left(1 - \left(\frac{DR_n}{DR_n + IC_{50,GRm}}\right)\right) - k_{d,GRm} \cdot GR_{m,mpl} \qquad IC = GR_{m,mpl}(0) \quad (9)$$

where the $IC_{50,GRm}$ is the concentration of DR_n at which the synthesis rate of GR mRNA is reduced to 50% of its baseline. Measures of GR mRNA expression (GR_m) following MPL dosing in adipose tissue (Sukumaran et al., 2011), lung, and skeletal muscle were used to infer the concentrations of free cytosolic receptor density (R) in those tissues based on Eq. (3).

Circadian Rhythm of GILZ mRNA Expression.

The GILZ mRNA displays circadian oscillations, which is under the complex regulation of CST as well as the peripheral circadian clock gene loop present in tissues (Ayyar et al., 2015; Soták et al., 2016). Circadian rhythms in GILZ mRNA expression in tissues were modeled using an IDR model with a time-dependent synthesis rate $k_{s,GILZm(t)}$, described by a single harmonic function and degraded by a first-order rate constant $k_{d,GILZm}$ as:

$$\frac{dGILZ_m}{dt} = k_{s,GILZm}(t) - k_{d,GILZm} \cdot GILZ_m \qquad IC = GILZ_m(0) \quad (10)$$

$$k_{s,GILZm}(t) = a_{0,GILZm} \cdot k_{d,GILZm} + \left(a_{1,GILZm} \cdot k_{d,GILZm} + \frac{2\pi b_{1,GILZm}}{24}\right) \cdot$$

$$cos\left(\frac{2\pi T}{24}\right) + \left(b_{1,GILZm} \cdot k_{d,GILZm} + \frac{2\pi a_{1,GILZm}}{24}\right) \cdot sin\left(\frac{2\pi T}{24}\right) \quad (11)$$

JPET Fast Forward. Published on July 20, 2017 as DOI: 10.1124/jpet.117.242990
This article has not been copyedited and formatted. The final version may differ from this version.

where a_i and b_i are Fourier coefficients associated with the harmonic oscillations. The values for these parameters were obtained by fitting the replicate GILZ mRNA expression data measured in tissues from the circadian control study using FOURPHARM.

Enhancement of GILZ mRNA Expression by CS

Transcriptional up-regulation of GILZ by CS has been documented in multiple cell types (D'Adamio et al., 1997; Eddleston et al., 2007; Aguilar et al., 2013). The pharmacogenomic effects of acute and chronic MPL dosing on GILZ mRNA expression in skeletal muscle, lung, and adipose tissue was modeled as a direct stimulation of the mRNA synthesis rate by the activated drug-receptor complex in the nucleus (DR_n) controlled by the stimulation constant, $S_{DRn}{}^{GILZm}$ as:

$$\frac{dGILZ_{m,mpl}}{dt} = k_{s,GILZm}(t) \cdot \left(1 + S_{DR_n}^{GILZm} \cdot DR_n\right) - k_{d,GILZm} \cdot GILZ_{m,mpl} \quad IC = GILZ_{m,mpl}(0) \qquad (12)$$

Data Analysis. The ADAPT 5 software was used for all data fitting and simulation of model equations (D'Argenio et al., 2009). The maximum likelihood method was applied for fitting the data. Replicate data at each time point from animals in each experiment were naïve-pooled, and data from both circadian control and single dose experiments were modeled simultaneously. Replicate data from the chronic MPL infusion study served as an external model validation set. The goodness-of-fit was assessed by system convergence, visual inspection of the fitted curves, objective function values such as Akaike Information Criterion (AIC), improved likelihood, examination of residuals, and precision (CV%) of the estimated parameters. The following variance model was used for the model fitting:

$$V_i = V(\theta, \sigma, t) = [\sigma_1 + \sigma_2 \cdot Y(\theta, t_i)]^2 \qquad (13)$$

where $V(\sigma,\theta,t_i)$ is the variance for the ith point, $Y(\theta,t_i)$ is the ith model-predicted value, θ represents the estimated structural parameters, and σ_1, σ_2 are the variance parameters that were estimated.

Animals in the dosing experiments were given MPL between 1.5 and 3 h after lights on. For simplicity, the dosing time was assumed to be at circadian time 2.5 h to compare the data obtained from both the

MPL-dosing and circadian experiments. Hence, all pharmacodynamic profiles are plotted with respect to circadian time with MPL given at 2.5 h.

Results

Pharmacokinetics

The plasma concentration-time profiles of MPL following IM bolus and SC infusion regimens are shown in Figure 4. The PK profile of IM-dosed MPL was simulated using parameter estimates obtained from a previously conducted PK study (Hazra et al., 2007b). MPL is known to undergo nonlinear interconversion as well as extensive hepatic oxidative metabolism in rats (Kong and Jusko, 1991). Further, plasma protein binding is relatively constant (f_{mpl} = 77%) with concentration (Haughey and Jusko, 1992). Steady-state concentrations of MPL in the infusion study were roughly 100-fold lower compared to those in previous bolus studies (Sun et al., 1998; Hazra et al., 2007b). Therefore, *CL* was estimated from the infusion data. The first sampling time in the infusion study was at 6 h after starting the infusion; by then MPL had achieved steady-state concentrations. Thus, the rising phase of the PK profile, which provides information regarding drug absorption and distribution was unavailable. Hence the distribution clearance and volumes of distribution were fixed based on the previous bolus estimates (Hazra et al., 2007b). In addition, drug absorption from the SC site was assumed to be complete and rapid compared to the rate of drug release from the pump. MPL clearance increased from 4.0 to 8.3 L/h/kg, which suggests that high concentrations of MPL cause saturation of drug-metabolizing enzymes. The PK parameters describing the data for both dosing regimens are listed in Table 1.

Circadian dynamics of GR mRNA expression

The daily fluctuation of receptor mRNA was examined in skeletal muscle and lung obtained from normal animals housed under tightly controlled 12-h light/12-h dark cycles. The profile for adipose tissue was simulated based on previous data collected from the same set of animals (Sukumaran et al., 2011). The circadian dynamics of tissue-specific GR mRNA along with the model fittings are presented in Figure 5.

Message expression in skeletal muscle (Figure 5) showed a modest circadian rhythm, starting at 1,164 ± 66 molecules/ng RNA in the light phase, with a nadir at the transition from the light-to-dark period (around 800 molecules/ng RNA) at 12 h, before gradually increasing through the dark period. This pattern was well

JPET Fast Forward. Published on July 20, 2017 as DOI: 10.1124/jpet.117.242990
This article has not been copyedited and formatted. The final version may differ from this version.

described by a single harmonic function. The baseline receptor mRNA expression was approximately 3-fold higher in lung compared to skeletal muscle (Figure 5). Furthermore, lung GR exhibited a circadian pattern distinct from muscle, showing a nadir in the light phase at 7 h, and a peak in the dark phase around 18 h, which was also adequately described by a single harmonic function. Interestingly, the observed patterns of receptor message in skeletal muscle and lung also varied from that observed in adipose tissue (Figure 5), where the circadian oscillations peaked at the transition from the light to dark period at time 12 h, which was described by a two-harmonic Fourier function (Sukumaran et al., 2011).

GR mRNA dynamics upon acute MPL dosing

Dynamics of GR mRNA expression following acute CS dosing was measured in muscle and lung, and simulated in adipose tissue based upon a previous report (Sukumaran et al., 2011). The dynamics of GR mRNA suppression in each tissue along with the model fittings are shown in Figure 6. MPL caused significant down-regulation in GR mRNA expression by 45 to 80% in skeletal muscle, lung, and adipose tissue with the nadirs occurring between 6-9 h after MPL dosing.

About 45 to 50% suppression in muscle receptor mRNA expression was observed at the nadir after MPL dosing, which returned to the rhythmic baseline by 24 h (Figure 6). The estimated degradation rate-constant ($k_{d,GRm}$) value of 0.28 h^{-1} (29.9 CV%) in skeletal muscle was higher than the value of 0.14 h^{-1} reported in muscle from ADX rats (Sun et al., 1999). The nadir occurred around 7-8 h after MPL versus 10-11 h in the ADX rats, which could be attributed to the higher $k_{d,GRm}$ in the normal animals. Acute MPL dosing led to about 60% suppression in lung GR mRNA at the nadir around 7-9 h and returned to baseline expression by 24 h after MPL (Figure 6), which was well described by the model. It can be noted that GR mRNA at the early time-points in the treatment group was higher than expression observed upon return to baseline after MPL, which was similar to GR expression in the circadian controls. The estimated degradation rate-constant ($k_{d,GRm}$) value of 0.26 h^{-1} (15.4 CV%) was similar to that obtained in skeletal muscle (0.28 h^{-1}) and in white adipose tissue (0.31 h^{-1}) (Sukumaran et al., 2011), but lower than the reported value of 0.12 h^{-1} in liver (Hazra et al., 2007a). Furthermore, the nadir in receptor mRNA expression after MPL dosing was

reached around the same time as in both muscle and adipose tissue, which could be attributed to similar $k_{d,GRm}$ values.

The suppression of GR mRNA expression by MPL in adipose tissue has been modeled previously (Sukumaran et al., 2011). Therefore, relevant parameter estimates were fixed to simulate the adipose tissue profile (Figure 6). Tissue-specific rates of receptor synthesis ($k_{s,GR}$) and free cytosolic receptor densities at baseline [*GR(0)*] were also estimated using the dynamics of GR mRNA expression in the tissues. Table 2 provides the parameter estimates related to GR dynamics.

Circadian dynamics of GILZ mRNA expression

Endogenous cyclic regulation of GILZ mRNA expression was examined in skeletal muscle, lung, and adipose obtained from normal untreated animals. The dynamics of circadian oscillations in GILZ mRNA expression in all three tissues along with the model fittings are shown in Figure 7. Superimposed on these figures is the profile of CST measured in plasma from the same animals. In all three tissues, GILZ mRNA regulation *in vivo* follows a pattern that is entrained to that of the CST rhythm.

Figure 7 shows the circadian mRNA expression profile of GILZ in skeletal muscle. Interestingly, a prominent delay in peak (9,330 ± 273 molecules/ng RNA) and trough (4,350 ± 743 molecules/ng RNA) expression was observed compared to lung and adipose tissue (Figure 7). Specifically, GILZ mRNA expression peaked at 20 h and showed a nadir around 9-10 h. The model well captured the trend of the circadian profile. In both lung and adipose, GILZ mRNA peaked in the dark period (18,867 ± 2,347 molecules/ng RNA for adipose and 25,202 ± 1,145 molecules/ng RNA for lung) at 16 h and showed a trough in the light period (4,446 ± 622 molecules/ng RNA for adipose and 5,141 ± 615 molecules/ng RNA for lung) around 6-8 h. Circadian rhythmicity in GILZ mRNA expression was strongest in lung compared to the other tissues. Although the model predicts peak expression around 17 h, the data are captured reasonably well by the single Fourier harmonic function.

GILZ mRNA dynamics upon acute MPL dosing

JPET Fast Forward. Published on July 20, 2017 as DOI: 10.1124/jpet.117.242990
This article has not been copyedited and formatted. The final version may differ from this version.

The CS such as dexamethasone cause strong up-regulation of GILZ mRNA expression *in vitro* (D'Adamio et al., 1997; Smit et al., 2005; Aguilar et al., 2013). Since basal expression of GILZ mRNA shows a circadian pattern *in vivo*, transcriptional enhancement of GILZ by exogenous CS must be interpreted within this context. As shown in Figure 8, the response of GILZ to MPL dosing clearly exceeded normal circadian variation in all tissues. Up-regulation of GILZ mRNA was observed as early as 15 minutes after dosing which continued to rise to peak values until as late as 8 hours, when plasma MPL concentrations continued to decline. GILZ mRNA eventually re-established its circadian rhythm in all tissues following perturbation by MPL. The estimated parameters for GILZ dynamics (Eq. 10-12) for all three tissues are provided in Table 3.

Figure 8 shows that GILZ mRNA is up-regulated in muscle, but to a lesser extent compared to lung and adipose. GILZ expression is enhanced 0.5 h after MPL dosing and sharply rises to its peak (15,851 ± 2598 molecules/ng RNA) by 5-6 h, which was earlier than peak times of GILZ in adipose tissue and lung. Conversely, the peak time of basal mRNA expression in muscle was delayed compared to that in adipose tissue and lung (Figure 7). In general, the model adequately captured the magnitude of up-regulation of GILZ by MPL as well as its return to circadian baseline, but it overestimated the time of peak response in muscle. This is likely due to the simultaneous fitting of the baseline profile along with the treatment dynamics, where an appreciable difference in times of peak expression were observed. The estimated $k_{d,GILZm}$ in muscle was 0.16 h^{-1} (14.3 CV%). The linear stimulatory constant of GILZ mRNA synthesis ($S_{DR_n}^{GILZm}$) in muscle was estimated as 0.27 nM^{-1} (40 CV%). GILZ mRNA expression was strongly up-regulated upon dosing with MPL in adipose showing a steady increase in expression starting as early as 30 min after MPL and reached its maximum around 8 h (55,053 ± 1,342 molecules/ng RNA), which was well described by the model. The estimated degradation constant of GILZ mRNA ($k_{d,GILZm}$) in adipose tissue was 0.21 h^{-1} (5.8 CV%), which corresponds to a turnover half-life of approximately 3.3 h. The estimated $S_{DR_n}^{GILZm}$ value of 0.3 nM^{-1} (8.3 CV%) in adipose was very similar to that in muscle. Drug-induced GILZ expression exceeded the amplitude of its baseline rhythm in lung by 2 h after dosing, and peaked around 8 h (41,952

± 1,519 molecules/ng RNA). The mRNA returned to baseline by 24 h, following which circadian rhythmicity was re-established. The model well-described the enhancement as well as the return to rhythmic baseline expression of GILZ upon acute MPL dosing. The estimated $k_{d,GILZm}$ value of 0.45 h^{-1} (7.7 CV%) indicated that the turnover half-life of GILZ mRNA is approximately 1.5 h in lung, about twice as rapid compared to adipose tissue. The $S_{DR_n}^{GILZm}$ in lung was estimated to be 0.47 nM^{-1} (6.8 CV%). Of interest, although the baseline oscillation of GILZ in lung was more robust than in adipose, the extent of MPL-mediated enhancement of GILZ mRNA from baseline in lung was lower.

GILZ mRNA dynamics upon chronic MPL dosing

The dynamic behavior of steroid-regulated genes can differ based upon the nature of the perturbation introduced within the system (Almon et al., 2007a). The time-course of GILZ mRNA expression was assessed in lung and adipose following an infusion of 0.3 mg/kg/h MPL over 7 days. The concentration-time profile for the chronic infusion was simulated based on the parameters in Table 1. The developed pharmacodynamic model was simulated using parameter values obtained for receptor and GILZ dynamics from Tables 2 and 3 to predict GILZ mRNA dynamics in lung and adipose tissue measured from these animals. Chronically elevated steroid concentrations disrupt or even abrogate the circadian rhythmicity of endogenous CST and tissue gene expression (Chung et al., 2011, Cole et al., 2000), and the significantly greater exogenous steroid would contribute more to stimulating target mRNA expression (Hazra et al, 2007). Thus the circadian rhythmicity for both GR and GILZ mRNA were not included for the chronic regimen and steady baselines were assumed. Simulations using the model and its parameters satisfactorily predicted the data patterns for both tissues.

The infusion of MPL produced a robust increase in GILZ mRNA in adipose tissue (Figure 9) with the peak expression reaching 59,720 ± 12,947 molecules/ng RNA at around 8-9 h. However, expression decreased from the peak to achieve a new steady-state despite the constant presence of drug, indicating a drug-induced tolerance phenomenon. The model captured the enhancement of GILZ mRNA upon chronic infusion and, more importantly, was able to accurately predict the steady-state dynamics achieved beyond 48 h and

throughout the 7-day infusion. A similar pattern of expression was observed in lung (Figure 9), with GILZ mRNA being enhanced to peak between 6-9 h after starting the infusion. Consistent with measurements from the acute dosing study, enhancement by MPL in lung was appreciably lower compared to adipose tissue. Expression in lung peaked at 31,692 ± 6,050 molecules/ng RNA and decreased to a steady-state of approximately 23,000 molecules/ng RNA, which was well captured by the model.

Simulation of receptor dynamics upon chronic MPL dosing

Several hypotheses exist for explaining the changes in steroid-regulated tissue gene expression after acute versus chronic dosing. It is possible that molecular events (receptor translocation, recycling, or chromatin binding) are altered during chronic dosing. Alternatively, signal transduction processes involved in generating the response can be amplified or diminished due to the chronic presence of steroid. Furthermore, secondarily-induced alterations in other hormones, such as insulin and glucagon, can influence the expression of responsive genes such as TAT and PEPCK upon chronic drug exposure (Holten and Kenney, 1967; Jin et al., 2004). In order to understand the molecular mechanisms governing the tolerance and tissue-specific GILZ dynamics observed with chronic dosing, we performed simulations of the GR mRNA, free cytosolic receptor (*R*), drug-receptor complex (*DR*), and nuclear drug-receptor complex (DR_n) in lung and adipose tissue (Figure 10).

While a rapid down-regulation of receptor mRNA was observed upon steroid exposure in both tissues, it took up to 24 h for attainment of steady-state. The model predicted a 50 to 55% decrease in GR mRNA expression from the controls in adipose tissue, which was similar to that observed in liver from chronically infused male ADX rats (Ramakrishnan et al., 2002b). The extent of down-regulation in lung was lower compared to adipose tissue, consistent with our observations in the acutely dosed animals. Cytosolic receptor density took as long as 48 h before achieving steady-state concentrations in both tissues. The simulated profile of *DR* concentrations in the cytosol showed a quick increase followed by a relatively rapid decrease to a lower steady-state in both tissues. The concentrations of DR_n present in the nucleus peaked at 3 h into the infusion, which followed the increase and return of *DR* complex to its own

steady-state, with a slight time delay. The time-course of these simulated GR dynamic profiles are in general agreement with previous chronic infusion studies assessing liver dynamics of ADX animals (Ramakrishnan et al., 2002a). The concentration of DR_n formation in adipose tissue was about 3-4 fold higher than DR_n in lung, which might conceivably explain the increased capacity for GILZ gene enhancement in adipose tissue versus lung.

Discussion

Despite increasing clinical use of targeted biologics for immune-related diseases, the CS remain a cornerstone in therapy owing to their widespread immunosuppressive effects. Among a few other transactivated genes, GILZ has been implicated in mediating anti-inflammatory CS effects (Ayroldi and Riccardi, 2009; Vandevyver et al., 2013). In this report, we sought to establish a mechanistic and quantitative basis using PK/PD modeling for the tissue-specific enhancement of GILZ by MPL under different dosing regimens *in vivo*.

The CS exert therapeutic and adverse effects in various organs via a coupled receptor-mediated mechanism. The catabolic effects of MPL dosing on organ weights display different sensitivities or capacity to respond to steroid treatment, which are dependent upon drug-receptor association and receptor densities within the tissues (Ramakrishnan et al., 2002b). Less is known regarding the precise mechanisms controlling differences in expression of a single or multiple genes across tissues. Here, we examine whether such tissue-specific regulation of GR control differences at the level of gene expression across tissues.

Endogenous glucocorticoid production from the adrenal cortex is regulated in a circadian fashion by the HPA axis via input from the suprachiasmatic nucleus, consequently producing oscillations in steroid-regulated genes in tissues. Such time-dependent variations in gene expression influences drug action, including pharmacodynamic responses, due to the availability or functioning of target proteins (Sukumaran et al., 2010). Hence, conclusions made from time-course studies require considering such oscillatory behaviors. All measures of GR and GILZ mRNA expression examined in our study displayed circadian oscillations. We examined the circadian regulation of GR mRNA and its dynamics after acute MPL dosing in skeletal muscle, lung, and adipose tissue. While it is not surprising to find that the amount of receptor mRNA expression varied across tissues, it was interesting to identify distinct, tissue-specific patterns of circadian rhythmicity, which can be of physiological importance. For example, the nadir of GR rhythmicity in skeletal muscle occurred at the transition from light-to-dark, which coincides with the time of peak plasma CST concentration. This pattern is in direct contrast to adipose tissue, where GR mRNA peaked at

the light-to-dark transition period. Such divergent tissue behavior may be explained from a standpoint of energy metabolism (Laposky et al., 2008). Since the animal is not feeding during the light/inactive period, it is dependent upon free fatty acid release from lipolysis as its main energy source, explaining a timely increase in GR expression to facilitate this process in adipose. Conversely, since glucocorticoids promote net protein degradation in muscle (Vegiopoulos and Herzig, 2007), decreased GR expression might serve as a protective mechanism against this effect. The circadian pattern of GR in lung was entrained to adrenal CST production, but the direct physiologic relevance of this behavior is not apparent. The MPL bolus dosing led to a rapid decrease in receptor mRNA in all three tissues, consistent with previous findings of tissue-specific GR mRNA regulation by dexamethasone (Kalinyak et al., 1987). The tissue dynamics followed relatively similar patterns over time, likely due to similar degradation rate constants.

The GILZ mRNA regulation in all three tissues followed a pattern that is entrained to the CST rhythm. CST, however, only partially controls the cyclic GILZ expression, since adrenalectomy does not completely abolish the circadian rhythm of GILZ mRNA in tissues (Sotak et al., 2016). Our results provide *in vivo* confirmation of prior *in vitro* studies (D'Adamio et al., 1997; Smit et al., 2005; Aguilar et al., 2013), showing that GILZ transcription is strongly enhanced upon CS exposure. The half-life of GILZ mRNA expression was estimated to be around 3-4 hours in muscle ($k_{d,GILZm}$ = 0.16 h^{-1}) and adipose tissue ($k_{d,GILZm}$ = 0.21 h^{-1}) and 1.5 hours in lung ($k_{d,GILZm}$ = 0.45 h^{-1}). Differences in mRNA degradation rate could arise from cell- or tissue-specific differences in cytoplasmic mRNA decay mechanisms (Linde et al., 2007; Schoenberg and Maquat, 2012). The concerted regulation of circadian rhythmicity and CS pharmacodynamics was apparent in lung and adipose tissue based upon simultaneous model fitting of the circadian and acute dosing profiles. The dynamics of GILZ in muscle, however, showed some divergence in the circadian and treatment profiles, which led to a discrepancy between the observed and model-estimated times of peak response in the treatment group. This could be caused by the direct tissue-specific effects of CS, where they produce an apparent phase-shift in response in peripheral clocks in intact animals (Balsalobre et al., 2000), which was not accounted for in this model. While we speculate that the higher sensitivity constant ($S_{DR_n}^{GILZm}$) in lung (beyond receptor differences) may arise due to the distinct primary

roles of CS in lung versus muscle and adipose (i.e. immune versus metabolic regulation), our findings based on *in vivo* measurements may provide some basis for further experimental assessments of this molecular process *in vitro*.

Chronic MPL produced a different dynamic behavior of GILZ expression compared to acute dosing. Prior microarray studies in muscle and liver following chronic MPL infusion indicated that various temporal patterns emerge for the drug-regulated genes (Almon et al., 2007a; Almon et al., 2007b). GILZ dynamics in both lung and adipose tissue showed a recognizable pattern where expression was rapidly enhanced to a peak, but then decreased over 24 h to achieve a new steady-state that was maintained until the end of the seven-day study period.

Quantitative systems modeling was employed to understand the dynamic mechanisms controlling tissue-specific MPL effects. Assuming the kinetics of drug entry into the tissues studied are not rate-limiting (i.e. well-perfused tissue entry), the dissociation constant for the drug-receptor binding and the free receptor density, as controlled by *de novo* receptor synthesis and degradation, the recycled fraction, and receptor mRNA autoregulation would limit the overall response of tissues to steroid treatment. We therefore measured the dynamics of GR message expression in the selected tissues and simulated tissue-specific free receptor densities using our model. The short half-life of MPL (~30 min) resulted in steady-state concentrations being achieved within a few hours during chronic infusion. However, simulation of lung and adipose tissue receptor dynamics showed that it takes at least 24 h for the steady-state to be attained, consistent with the time-course of receptor measures in ADX liver (Ramakrishnan et al., 2002b). The fifth-generation model captured GILZ dynamics in both tissues, while demonstrating that receptor down-regulation was the common mechanism controlling the tolerance in pharmacogenomic responses. Also demonstrated was that tissue-specific concentrations of the steroid-receptor complex (DR_n) corresponded with the capacity of MPL-mediated GILZ enhancement in those tissues. Interestingly, the same model indicated that post-receptor events contributed to a decoupling between receptor dynamics and hepatic TAT gene induction during long-term dosing, attributed to secondarily-induced changes in insulin, which also regulates TAT (Ramakrishnan et al., 2002b). Our model simulations suggest that certain parameters such

as k_{on}, k_{re}, k_t, and R_f, fixed based on bolus dose estimates to constant values across the tissues, are less likely to influence the divergence in the tissue- and dosage regimen-dependent behaviors of GILZ *in vivo*.

A salient feature of this study is that replicate data obtained from both circadian and MPL experiments were modeled jointly to obtain parameter values. Despite the model being developed based on a single dose and using a linear stimulation coefficient ($S_{DR_n}^{GILZm}$) instead of a more appropriate saturable effect function, the final model well-predicted GILZ dynamics upon chronic steroid exposure. A limitation is the assumption of a normal CST rhythm in acutely dosed animals. In reality, MPL causes suppression of endogenous CST by binding to GR in the pituitary, thereby modulating its release from the adrenal cortex (Cole et al., 2000; Yao et al., 2008). This, in turn, could modulate endogenous GILZ expression. However, MPL binds GR with higher affinity than CST, predominantly exerting receptor/gene-mediated effects when present in the system. Furthermore, adrenalectomy dampens the amplitude but does not abolish circadian GILZ expression in tissues (Sotak et al., 2016), possibly indicating an added regulatory mechanism involving peripheral clock genes. Since inclusion of these processes without additional data would have resulted in over-parameterization, a semi-mechanistic IDR approach based on Fourier harmonics was utilized to describe the non-stationarity in baselines.

These studies quantitatively assess CS kinetics, dynamics, and genomics on the molecular and tissue levels while accounting for circadian rhythms, providing a physiologically integrated examination of how multiple factors interact to control the *in vivo* responses to an important class of therapeutic agents. These studies lay the foundation to investigate sex differences in the PK/PD response to CS employing GILZ as a biomarker (Whirledge and Cidlowski, 2013). Also of importance would be to examine the regulation of GILZ in animal models of inflammatory disease (Earp et al., 2009), since GILZ is an anti-inflammatory mediator in RA (Beaulieu et al., 2010). Enhanced pharmacodynamic models are being applied to provide a deeper understanding of drug action from molecular to whole system responses (Iyengar et al., 2012; Jusko, 2013). The present findings of tissue-specific differences in basal and drug-induced expression and their controlling mechanisms indicate that such factors should be considered in

view of the dose, pharmacokinetics, pharmacodynamics, and target organ actions for drugs acting through genomic mechanisms.

Authorship contributions

Participated in research design: Ayyar, DuBois, Almon, and Jusko

Conducted experiments: Ayyar and DuBois

Performed data analysis: Ayyar and Jusko

Wrote or contributed to the writing of the manuscript: Ayyar, DuBois, Almon, and Jusko

References

Aguilar DC, Strom J, Xu B, Kappeler K and Chen QM (2013) Expression of glucocorticoid-induced leucine zipper (GILZ) in cardiomyocytes. *Cardiovasc Toxicol* **13**:91-99.

Almon RR, Dubois DC, Jin JY and Jusko WJ (2005a) Pharmacogenomic responses of rat liver to methylprednisolone: an approach to mining a rich microarray time series. *AAPS J* **7**:E156-194.

Almon RR, DuBois DC and Jusko WJ (2007a) A microarray analysis of the temporal response of liver to methylprednisolone: a comparative analysis of two dosing regimens. *Endocrinology* **148**:2209-2225.

Almon RR, DuBois DC, Yao Z, Hoffman EP, Ghimbovschi S and Jusko WJ (2007b) Microarray analysis of the temporal response of skeletal muscle to methylprednisolone: comparative analysis of two dosing regimens. *Physiol Genomics* **30**:282-299.

Almon RR, Lai W, DuBois DC and Jusko WJ (2005b) Corticosteroid-regulated genes in rat kidney: mining time series array data. *Am J Physiol Endocrinol Metab* **289**:E870-882.

Almon RR, Yang E, Lai W, Androulakis IP, DuBois DC and Jusko WJ (2008) Circadian variations in rat liver gene expression: relationships to drug actions. *J Pharmacol Exp Ther* **326**:700-716.

Ayroldi E, Petrillo MG, Bastianelli A, Marchetti MC, Ronchetti S, Nocentini G, Ricciotti L, Cannarile L and Riccardi C (2015) L-GILZ binds p53 and MDM2 and suppresses tumor growth through p53 activation in human cancer cells. *Cell Death Differ* **22**:118-130.

Ayroldi E and Riccardi C (2009) Glucocorticoid-induced leucine zipper (GILZ): a new important mediator of glucocorticoid action. *FASEB J* **23**:3649-3658.

Ayyar VS, Almon RR, Jusko WJ and DuBois DC (2015) Quantitative tissue-specific dynamics of in vivo GILZ mRNA expression and regulation by endogenous and exogenous glucocorticoids. *Physiol Rep* **3**:pii: e12382.

Balsalobre A, Brown SA, Marcacci L, Tronche F, Kellendonk C, Reichardt HM, Schütz G and Schibler U (2000) Resetting of circadian time in peripheral tissues by glucocorticoid signaling. *Science* **289**:2344.

Barnes PJ (1998) Efficacy of inhaled corticosteroids in asthma. *J Allergy Clin Immunol* **102**:531-538.

Barnes PJ (2006) How corticosteroids control inflammation: Quintiles Prize Lecture 2005. *Br J Pharmacol* **148**:245-254.

Beaulieu E, Ngo D, Santos L, Yang YH, Smith M, Jorgensen C, Escriou V, Scherman D, Courties G, Apparailly F and Morand EF (2010) Glucocorticoid-induced leucine zipper is an endogenous antiinflammatory mediator in arthritis. *Arthritis Rheum* **62**:2651-2661.

Bruscoli S, Biagioli M, Sorcini D, Frammartino T, Cimino M, Sportoletti P, Mazzon E, Bereshchenko O and Riccardi C (2015) Lack of glucocorticoid-induced leucine zipper (GILZ) deregulates B-cell survival and results in B-cell lymphocytosis in mice. *Blood* **126**:1790-1801.

Bustin SA, Benes V, Garson JA, Hellemans J, Huggett J, Kubista M, Mueller R, Nolan T, Pfaffl MW, Shipley GL, Vandesompele J and Wittwer CT (2009) The MIQE guidelines: minimum information for publication of quantitative real-time PCR experiments. *Clin Chem* **55**:611-622.

Cannarile L, Zollo O, D'Adamio F, Ayroldi E, Marchetti C, Tabilio A, Bruscoli S and Riccardi C (2001) Cloning, chromosomal assignment and tissue distribution of human GILZ, a glucocorticoid hormone-induced gene. *Cell Death Differ* **8**:201-203.

Chung S, Son GH and Kim K (2011) Circadian rhythm of adrenal glucocorticoid: Its regulation and clinical implications. *Biochimica et Biophysica Acta (BBA) - Molecular Basis of Disease* **1812**:581-591.

Cole MA, Kim PJ, Kalman BA and Spencer RL (2000) Dexamethasone suppression of corticosteroid secretion: evaluation of the site of action by receptor measures and functional studies. *Psychoneuroendocrinology* **25**:151-167.

D'Adamio F, Zollo O, Moraca R, Ayroldi E, Bruscoli S, Bartoli A, Cannarile L, Migliorati G and Riccardi C (1997) A new dexamethasone-induced gene of the leucine zipper family protects T lymphocytes from TCR/CD3-activated cell death. *Immunity* **7**:803-812.

D'Argenio D, Schumitzky A and Wang X (2009) ADAPT 5 User's Guide: Pharmacokinetic/Pharmacodynamic Systems Analysis Software, in, BioMedical Simulations Resource, Los Angeles.

Di Marco B, Massetti M, Bruscoli S, Macchiarulo A, Di Virgilio R, Velardi E, Donato V, Migliorati G and Riccardi C (2007) Glucocorticoid-induced leucine zipper (GILZ)/NF-kappaB interaction: role of GILZ homo-dimerization and C-terminal domain. *Nucleic Acids Res* **35**:517-528.

DuBois DC, Xu ZX, McKay L, Almon RR, Pyszcznski N and Jusko WJ (1995) Differential dynamics of receptor down-regulation and tyrosine aminotransferase induction following glucocorticoid treatment. *J Steroid Biochem Mol Biol* **54**:237-243.

Earp JC, Dubois DC, Almon RR and Jusko WJ (2009) Quantitative dynamic models of arthritis progression in the rat. *Pharm Res* **26**:196-203.

Eddleston J, Herschbach J, Wagelie-Steffen AL, Christiansen SC and Zuraw BL (2007) The anti-inflammatory effect of glucocorticoids is mediated by glucocorticoid-induced leucine zipper in epithelial cells. *J Allergy Clin Immunol* **119**:115-122.

Haughey DB and Jusko WJ (1988) Analysis of methylprednisolone, methylprednisone and corticosterone for assessment of methylprednisolone disposition in the rat. *J Chromatogr* **430**:241-248.

Haughey DB and Jusko WJ (1992) Bioavailability and nonlinear disposition of methylprednisolone and methylprednisone in the rat. *J Pharm Sci* **81**:117-121.

Hazra A, Pyszczynski N, DuBois DC, Almon RR and Jusko WJ (2007a) Modeling receptor/gene-mediated effects of corticosteroids on hepatic tyrosine aminotransferase dynamics in rats: dual regulation by endogenous and exogenous corticosteroids. *J Pharmacokinet Pharmacodyn* **34**:643-667.

Hazra A, Pyszczynski N, DuBois DC, Almon RR and Jusko WJ (2007b) Pharmacokinetics of methylprednisolone after intravenous and intramuscular administration in rats. *Biopharm Drug Dispos* **28**:263-273.

Hazra A, Pyszczynski NA, DuBois DC, Almon RR and Jusko WJ (2008) Modeling of corticosteroid effects on hepatic low-density lipoprotein receptors and plasma lipid dynamics in rats. *Pharm Res* **25**:769-780.

Holten D and Kenney FT (1967) Regulation of tyrosine alpha-ketoglutarate transaminase in rat liver. VI. Induction by pancreatic hormones. *J Biol Chem* **242**:4372-4377.

Iyengar R, Zhao S, Chung S-W, Mager DE and Gallo JM (2012) Merging systems biology with pharmacodynamics. *Sci Transl Med* **4**:126ps7.

Jin JY, DuBois DC, Almon RR and Jusko WJ (2004) Receptor/gene-mediated pharmacodynamic effects of methylprednisolone on phosphoenolpyruvate carboxykinase regulation in rat liver. *J Pharmacol Exp Ther* **309**:328-339.

Jusko WJ (1995) Pharmacokinetics and receptor-mediated pharmacodynamics of corticosteroids. *Toxicology* **102**:189-196.

Jusko WJ (2013) Moving from basic toward systems pharmacodynamic models. *J Pharm Sci* **102**:2930-2940.

Kalinyak JE, Dorin RI, Hoffman AR and Perlman AJ (1987) Tissue-specific regulation of glucocorticoid receptor mRNA by dexamethasone. *J Biol Chem* **262**:10441-10444.

Kirwan JR (1995) The effect of glucocorticoids on joint destruction in rheumatoid arthritis. *N Engl J Med* **333**:142-147.

Kofman S, Perlia CP, Boesen E, Eisenstein R and Taylor SG (1962) The role of corticosteroids in the treatment of malignant lymphomas. *Cancer* **15**:338-345.

Kong AN and Jusko WJ (1991) Disposition of methylprednisolone and its sodium succinate prodrug in vivo and in perfused liver of rats: nonlinear and sequential first-pass elimination. *J Pharm Sci* **80**:409-415.

Krzyzanski W, Chakraborty A and Jusko WJ (2000) Algorithm for application of Fourier analysis for biorhythmic baselines of pharmacodynamic indirect response models. *Chronobiol Int* **17**:77-93.

Laposky AD, Bass J, Kohsaka A and Turek FW (2008) Sleep and circadian rhythms: Key components in the regulation of energy metabolism. *FEBS Letters* **582**:142-151.

Linde L, Boelz S, Neu-Yilik G, Kulozik AE and Kerem B (2007) The efficiency of nonsense-mediated mRNA decay is an inherent character and varies among different cells. *Eur J Hum Genet* **15**:1156-1162.

Newton R (2000) Molecular mechanisms of glucocorticoid action: what is important? *Thorax* **55**:603-613.

Oakley RH and Cidlowski JA (1993) Homologous down regulation of the glucocorticoid receptor: the molecular machinery. *Crit Rev Eukaryot Gene Expr* **3**:63-88.

Pratt WB and Toft DO (1997) Steroid receptor interactions with heat shock protein and immunophilin chaperones. *Endocr Rev* **18**:306-360.

Ramakrishnan R, DuBois DC, Almon RR, Pyszczynski NA and Jusko WJ (2002a) Fifth-generation model for corticosteroid pharmacodynamics: application to steady-state receptor down-regulation and

enzyme induction patterns during seven-day continuous infusion of methylprednisolone in rats. *J Pharmacokinet Pharmacodyn* **29**:1-24.

Ramakrishnan R, DuBois DC, Almon RR, Pyszczynski NA and Jusko WJ (2002b) Pharmacodynamics and pharmacogenomics of methylprednisolone during 7-day infusions in rats. *J Pharmacol Exp Ther* **300**:245-256.

Schoenberg DR and Maquat LE (2012) Regulation of cytoplasmic mRNA decay. *Nat Rev Genet* **13**:246-259.

Smit P, Russcher H, de Jong FH, Brinkmann AO, Lamberts SW and Koper JW (2005) Differential regulation of synthetic glucocorticoids on gene expression levels of glucocorticoid-induced leucine zipper and interleukin-2. *J Clin Endocrinol Metab* **90**:2994-3000.

Sotak M, Bryndova J, Ergang P, Vagnerova K, Kvapilova P, Vodicka M, Pacha J and Sumova A (2016) Peripheral circadian clocks are diversely affected by adrenalectomy. *Chronobiol Int* **33**:520-529.

Sukumaran S, Almon RR, DuBois DC and Jusko WJ (2010) Circadian rhythms in gene expression: Relationship to physiology, disease, drug disposition and drug action. *Adv Drug Deliv Rev* **62**:904-917.

Sukumaran S, Jusko WJ, DuBois DC and Almon RR (2011) Mechanistic modeling of the effects of glucocorticoids and circadian rhythms on adipokine expression. *J Pharmacol Exp Ther* **337**:734-746.

Sun YN, DuBois DC, Almon RR, Pyszczynski NA and Jusko WJ (1998) Dose-dependence and repeated-dose studies for receptor/gene-mediated pharmacodynamics of methylprednisolone on glucocorticoid receptor down-regulation and tyrosine aminotransferase induction in rat liver. *J Pharmacokinet Biopharm* **26**:619-648.

Sun YN, McKay LI, DuBois DC, Jusko WJ and Almon RR (1999) Pharmacokinetic/Pharmacodynamic models for corticosteroid receptor down-regulation and glutamine synthetase induction in rat skeletal muscle by a receptor/gene-mediated mechanism. *J Pharmacol Exp Ther* **288**:720-728.

Van Cantfort J and Gielen JE (1979) Comparison of rat and mouse circadian rhythm of cholesterol-7 alpha-hydroxylase activity. *J Steroid Biochem* **10**:647-651.

Van der Laan S, Sarabdjitsingh RA, Van Batenburg MF, Lachize SB, Li H, Dijkmans TF, Vreugdenhil E, de Kloet ER and Meijer OC (2008) Chromatin immunoprecipitation scanning identifies

glucocorticoid receptor binding regions in the proximal promoter of a ubiquitously expressed glucocorticoid target gene in brain. *J Neurochem* **106**:2515-2523.

Vandevyver S, Dejager L, Tuckermann J and Libert C (2013) New insights into the anti-inflammatory mechanisms of glucocorticoids: an emerging role for glucocorticoid-receptor-mediated transactivation. *Endocrinology* **154**:993-1007.

Vegiopoulos A and Herzig S (2007) Glucocorticoids, metabolism and metabolic diseases. *Mol Cell Endocrinol* **275**:43-61.

Whirledge S and Cidlowski JA (2013) Estradiol antagonism of glucocorticoid-induced GILZ expression in human uterine epithelial cells and murine uterus. *Endocrinology* **154**:499-510.

Yao Z, DuBois DC, Almon RR and Jusko WJ (2008) Pharmacokinetic/pharmacodynamic modeling of corticosterone suppression and lymphocytopenia by methylprednisolone in rats. *J Pharm Sci* **97**:2820-2832.

Footnotes

This work was supported by the National Institute of General Medical Sciences, National Institutes of Health [Grant GM24211].

Figure Legends

Figure 1. Pharmacokinetic model for methylprednisolone with dose input either as an intramuscular injection (IM) or a subcutaneous infusion (SC); the symbols are defined in the text and Table 1. The model is described by Equations 1 and 2.

Figure 2. Schematic representation of diverse molecular and cellular mechanisms of corticosteroid action on regulating gene expression. CBG, corticosteroid-binding globulin; hsp 70/90, heat shock protein 70/90; FKBP, FK506 binding protein; GR, glucocorticoid receptor; nGRE, negative-glucocorticoid response element; GILZ, glucocorticoid-induced leucine zipper; RNAP, RNA polymerase.

Figure 3. PK/PD model schematic for the pharmacogenomic effects of corticosteroids and circadian rhythms on the transcriptional regulation of GILZ mRNA expression. Curved input represents circadian pattern in production, open boxes reflect stimulation, and solid boxes depict inhibition of production rate of a turnover process. The model is described by Equations 3 to 12. Parameters are defined in Tables 2 and 3.

Figure 4. Methylprednisolone (MPL) pharmacokinetics in rats. Simulated plasma concentrations versus time after 50 mg/kg IM injection of MPL using Equations 1 and 2. Pharmacokinetics of MPL upon administration of 0.3 mg/kg/h infusions for 7 days. Solid lines represent model fittings, and circles depict mean and error bars one standard deviation (n=3).

Figure 5. Circadian rhythm of glucocorticoid receptor (GR) mRNA expression in three tissues from baseline-control animals. Circles represent mean and error bars one standard deviation (n=3). The solid line depicts the fitting results using the PK/PD model depicted in Figure 3. Unshaded regions depict light phase and shaded regions dark phase of the 24-hour cycle.

Figure 6. Glucocorticoid receptor (GR) mRNA expression in three tissues from rats given 50 mg/kg IM MPL. Circles represent mean and error bars one standard deviation (n=3). The solid line depicts the fitting using the PK/PD model depicted in Figure 3 using parameter estimates listed in Table 2.

Figure 7. Circadian rhythm of GILZ mRNA expression in three tissues from baseline-control animals. Circles represent mean and error bars one standard deviation (n=3). The solid line depicts the fitting results using the PK/PD model depicted in Figure 3. The dashed line represents plasma corticosterone measurements from the same animals.

Figure 8. GILZ mRNA expression in three tissues from rats given 50 mg/kg IM MPL. Circles represent mean and error bars one standard deviation (n=3) The solid lines show model fittings (Figure 3) using parameter estimates listed in Table 3.

Figure 9. GILZ mRNA expression in lung and adipose tissue from rats infused with 0.3 mg/kg/h SC MPL for 7 days. Solid circles represent experimental data from individual rats and solid lines are simulations using the PK/PD model depicted in Figure 3. The parameters used are those for acute steroid effects listed in Table 3.

Figure 10. Simulated profiles of the driving forces (GR mRNA, free cytosolic receptor, and drug-receptor complex in the cytosol and nucleus) controlling GILZ regulation in lung and adipose tissue from rats infused with 0.3 mg/kg/h MPL for 7 days. Simulations are based on the model in Figure 3. The parameters are those for acute MPL effects as listed in Tables 2 and 3.

JPET Fast Forward. Published on July 20, 2017 as DOI: 10.1124/jpet.117.242990
This article has not been copyedited and formatted. The final version may differ from this version.

TABLE 1. Pharmacokinetic parameters of methylprednisolone.

Parameter	Definition	Estimate (CV%)
F	Bioavailability	$0.214^{a,b}$ / 1.0^{c}
Fr	Fraction absorbed by k_{a1}	$0.73^{a,b}$ / NA^{c}
k_{a1} (h^{-1})	Absorption rate constant	$1.26^{a,b}$ / NA^{c}
k_{a2} (h^{-1})	Absorption rate constant	$0.22^{a,b}$ / NA^{c}
V_P (mL/kg)	Plasma volume of distribution	$718.7^{a,b,c}$
V_T (mL/kg)	Tissue volume of distribution	$913.5^{a,b,c}$
CL_D (L/h/kg)	Distribution clearance	$2.6^{a,b,c}$
CL (L/h/kg)	Clearance	$4.0^{a,b}$ / 8.3^{c} (10.1)

[a] IM parameter values fixed from Hazra et al. 2007b

[b] 50 mg/kg IM bolus; [c] 0.3 mg/kg/h SC infusion

JPET Fast Forward. Published on July 20, 2017 as DOI: 10.1124/jpet.117.242990
This article has not been copyedited and formatted. The final version may differ from this version.

TABLE 2. Parameter values for GR mRNA expression and receptor dynamics.

Parameter	Definition	Estimate (CV%)
$a_{0,GRm}$	Fourier coefficient for GR mRNA	2824[c] / 1055.9[d] / 2216[a,e]
$a_{1,GRm}$	Fourier coefficient for GR mRNA	6.8[c] / 162.2[d] / -273.2[a,e]
$a_{2,GRm}$	Fourier coefficient for GR mRNA	65.9 [a,e]
$b_{1,GRm}$	Fourier coefficient for GR mRNA	185.6[c] / -19.9[d] / -10.9[a,e]
$b_{2,GRm}$	Fourier coefficient for GR mRNA	10.1 [a,e]
$k_{d,GRm}$ (h^{-1})	Degradation rate constant for GR mRNA	0.26 (15.4)[c] / 0.28[d] (29.9) / 0.31[a,e]
$k_{s,GR}$ (nM/h)(mol/ng)$^{-1}$	Synthesis rate constant for receptor	0.00025 (5.3)[c] / 0.00121[d] (34.5) / 00196[a,e]
$IC_{50,GRm}$ (nM^{-1})	Inhibition of GR mRNA production	15.6 [b]
$k_{d,GR}$ (h^{-1})	Degradation rate constant for receptor	0.05 [b]
k_{on} ($nM^{-1}\cdot h^{-1}$)	Association rate constant	0.016 [b]
f_{mpl}	Unbound fraction of MPL in plasma	0.23 [b]
k_{re} (h^{-1})	DR_n loss rate constant	1.31 [b]
R_f	Fraction recycled	0.93 [b]
k_T (h^{-1})	Translocation rate constant	58.3 [b]
$GR_{m,MPL}(0)$ (mol/ng RNA)	GR mRNA initial concentration (treatment)	4000 (fixed)[c] / 1350[d] (10.7) / 2200[a,e]
$GR(0)$ (nM)	Free cytosolic receptor initial concentration	19.7 (5.3)[c] / 32.7[d] (34.5) / 86.2[a,e]
$DR(0)$ (nM)	Drug-receptor complex initial concentration	0 (fixed)
$DR_n(0)$ (nM)	Nuclear complex initial concentration	0 (fixed)

[a] Parameter values fixed from Sukumaran et al. 2011

[b] Parameter values fixed from Hazra et al. 2007a

[c] Lung; [d] Muscle; [e] Adipose tissue

JPET Fast Forward. Published on July 20, 2017 as DOI: 10.1124/jpet.117.242990
This article has not been copyedited and formatted. The final version may differ from this version.

TABLE 3. Parameter values for the dynamics of GILZ mRNA expression.

Parameter	Definition	Estimate (CV%)
$a_{0,GILZm}$	Fourier coefficient for GILZ mRNA	14002[a] / 6479[b] / 9845[c]
$a_{1,GILZm}$	Fourier coefficient for GILZ mRNA	-3447[a] / 1133[b] / -441[c]
$b_{1,GILZm}$	Fourier coefficient for GILZ mRNA	-8339[a] / -1651[b] / -5148[c]
$k_{d,GILZm}$ (h^{-1})	Degradation rate constant for GILZ mRNA	0.45[a] (7.7) / 0.16[b] (14.3) / 0.21[c] (5.8)
S_{DRn}^{GILZm} (nM^{-1})	Stimulation of GILZ mRNA production	0.47[a] (6.8) / 0.27[b] (40.0) / 0.3[c] (8.3)
$GILZ_{mMPL}(0)$ (mol/ng RNA)	GILZ mRNA initial concentration (treatment)	10560[a] (fixed) / 4249[b] (17.9) / 6077[c] (21.3)

[a] Lung; [b] Muscle; [c] Adipose tissue

JPET Fast Forward. Published on July 20, 2017 as DOI: 10.1124/jpet.117.242990
This article has not been copyedited and formatted. The final version may differ from this version.

Figures

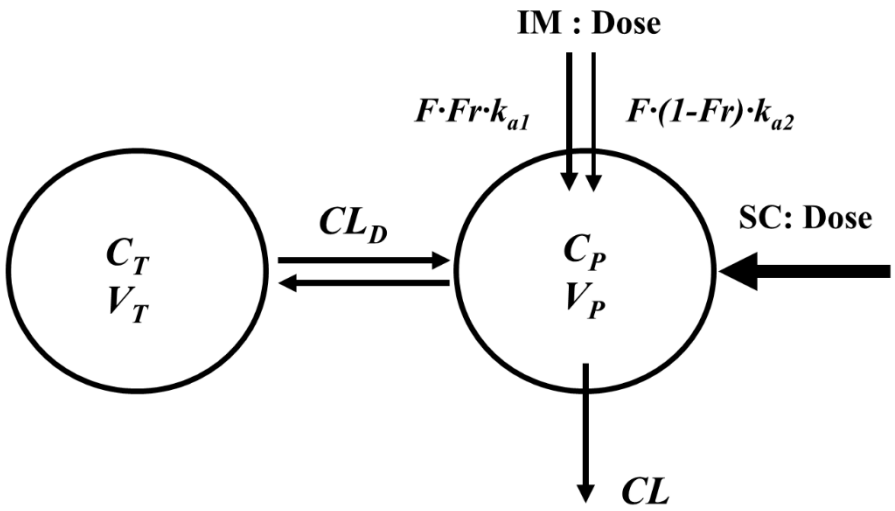

Figure 1

JPET Fast Forward. Published on July 20, 2017 as DOI: 10.1124/jpet.117.242990
This article has not been copyedited and formatted. The final version may differ from this version.

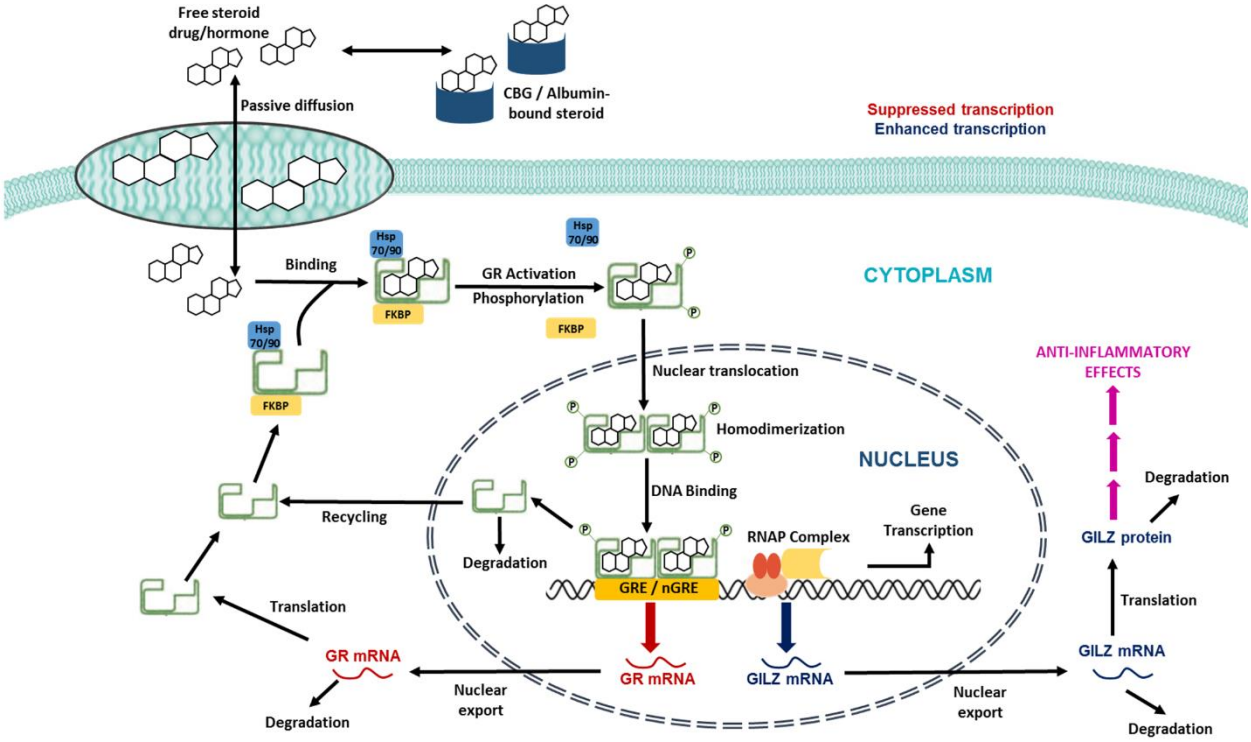

Figure 2

JPET Fast Forward. Published on July 20, 2017 as DOI: 10.1124/jpet.117.242990
This article has not been copyedited and formatted. The final version may differ from this version.

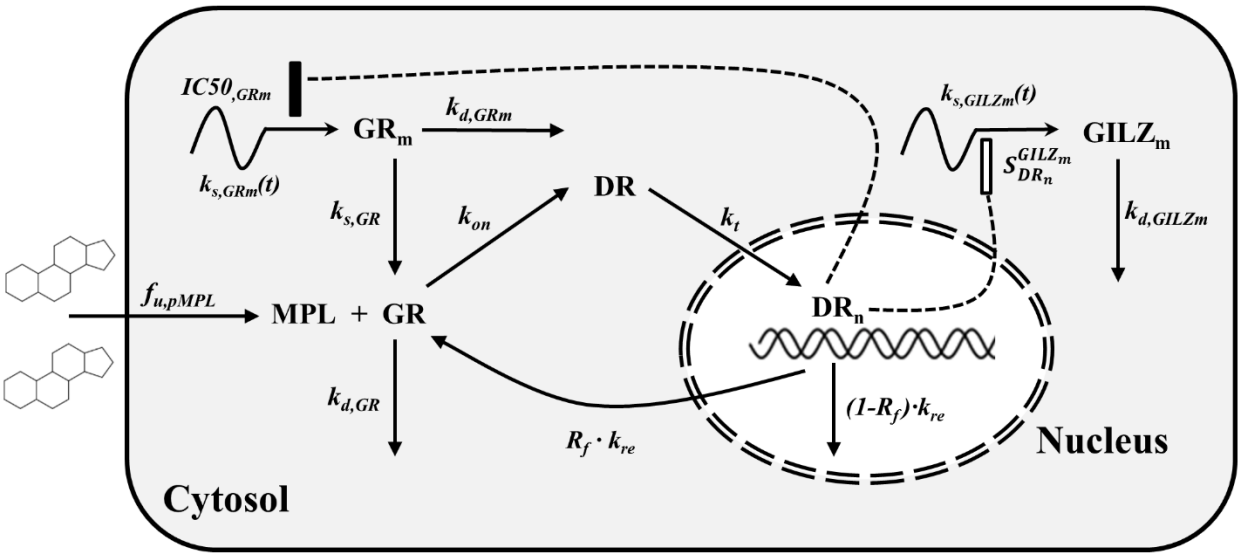

Figure 3

JPET Fast Forward. Published on July 20, 2017 as DOI: 10.1124/jpet.117.242990
This article has not been copyedited and formatted. The final version may differ from this version.

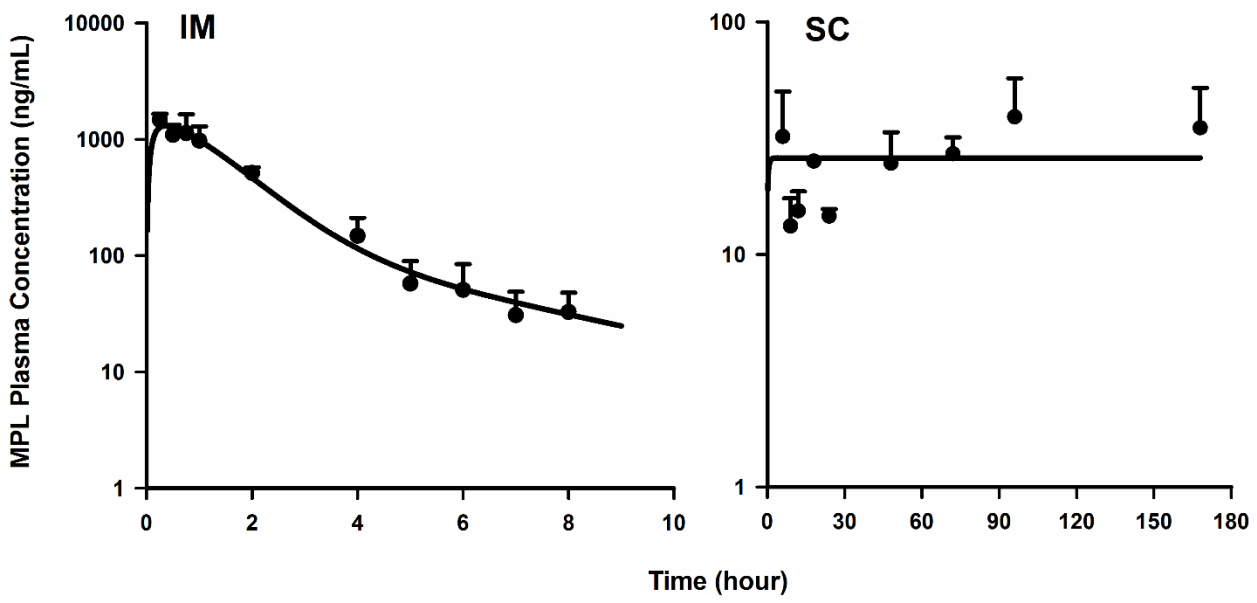

Figure 4

JPET Fast Forward. Published on July 20, 2017 as DOI: 10.1124/jpet.117.242990
This article has not been copyedited and formatted. The final version may differ from this version.

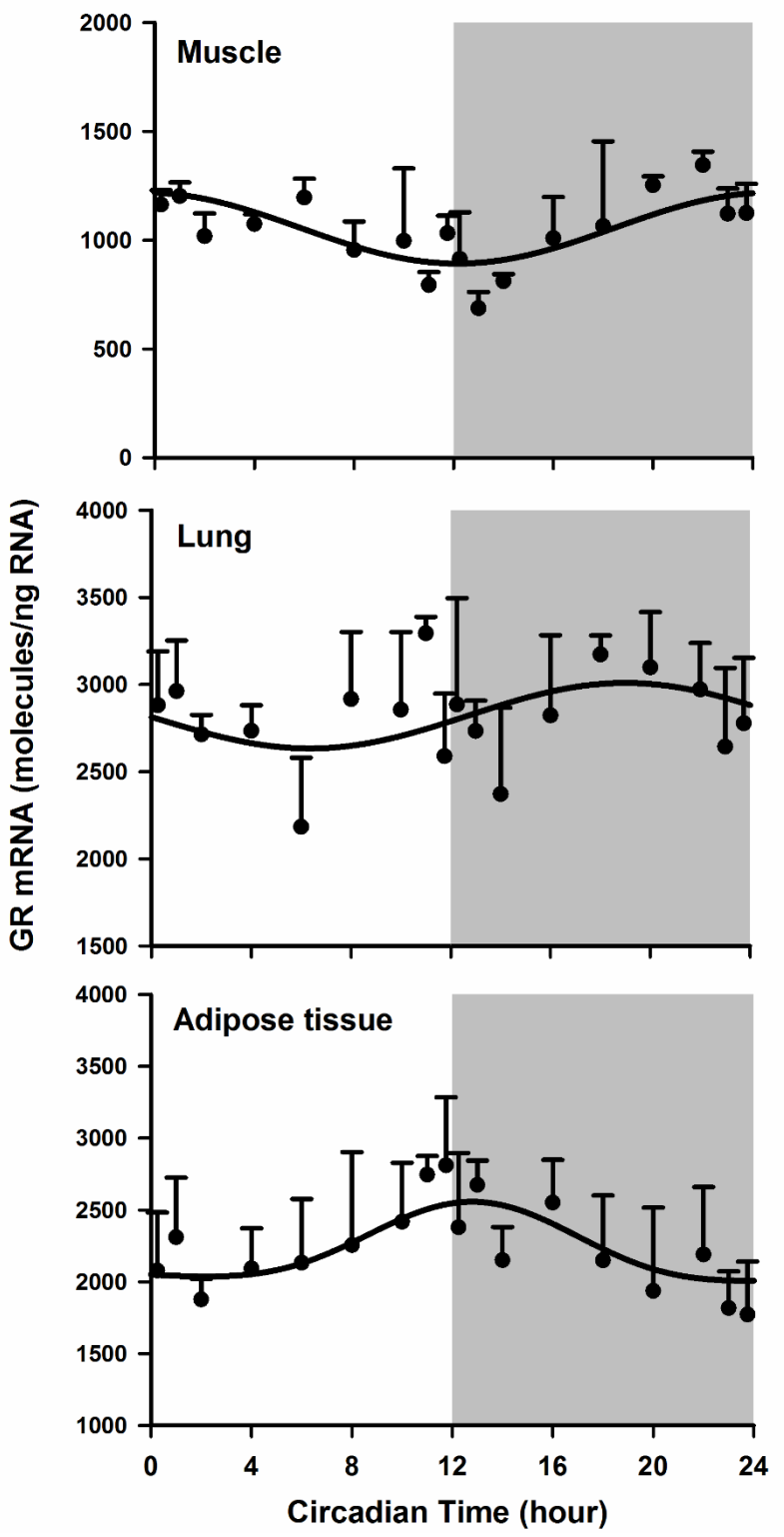

Figure 5

JPET Fast Forward. Published on July 20, 2017 as DOI: 10.1124/jpet.117.242990
This article has not been copyedited and formatted. The final version may differ from this version.

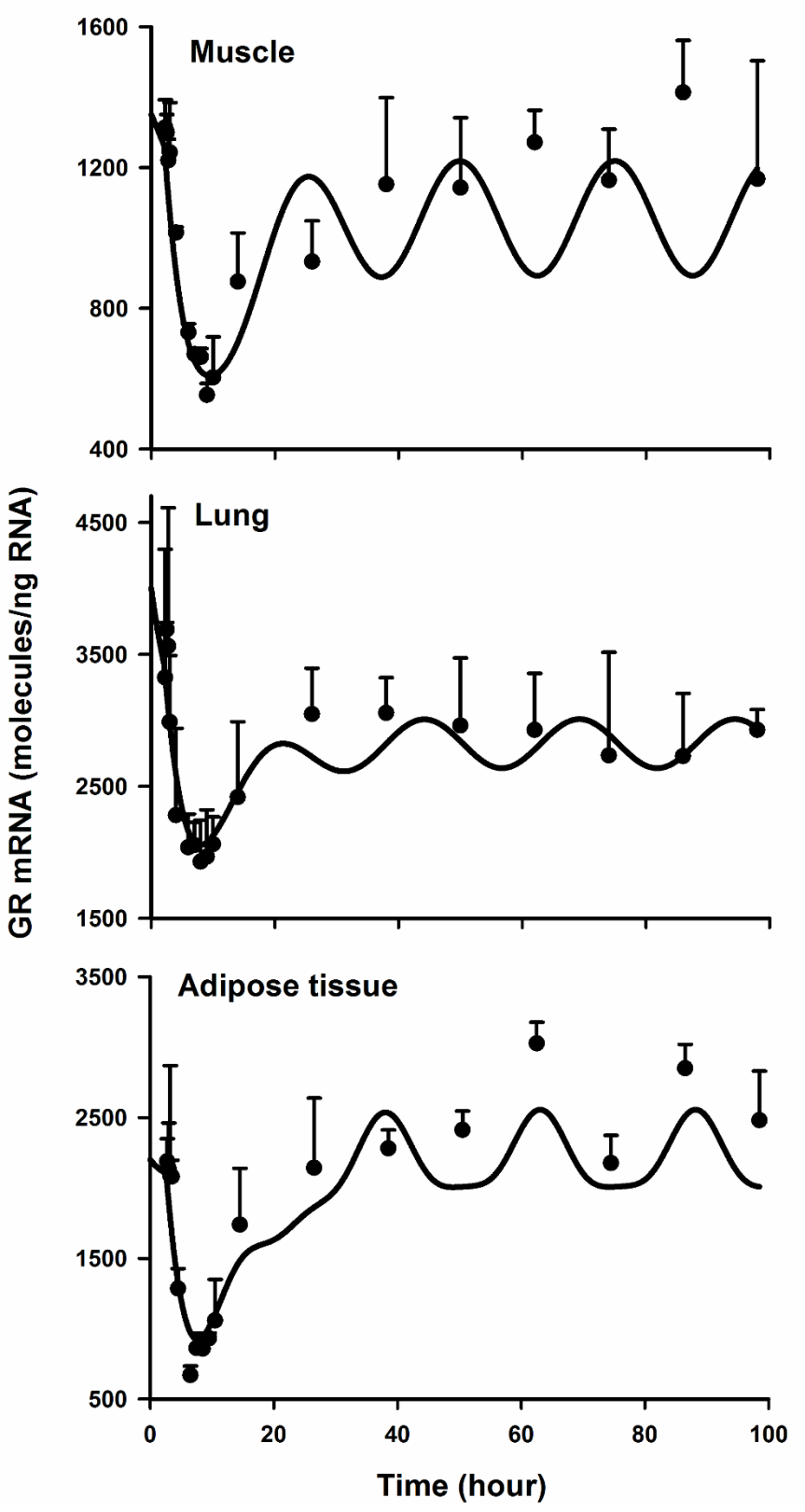

Figure 6

JPET Fast Forward. Published on July 20, 2017 as DOI: 10.1124/jpet.117.242990
This article has not been copyedited and formatted. The final version may differ from this version.

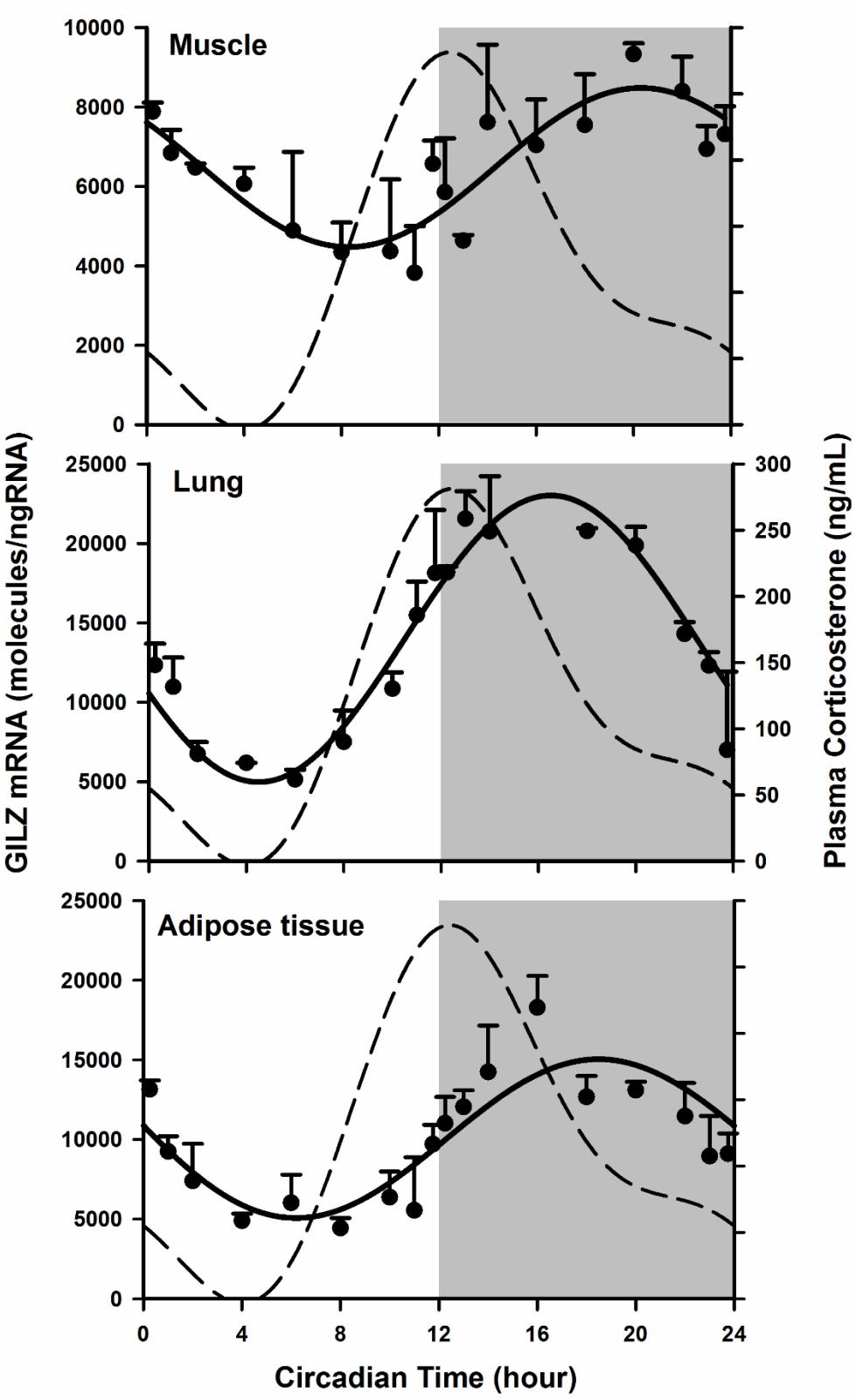

Figure 7

JPET Fast Forward. Published on July 20, 2017 as DOI: 10.1124/jpet.117.242990
This article has not been copyedited and formatted. The final version may differ from this version.

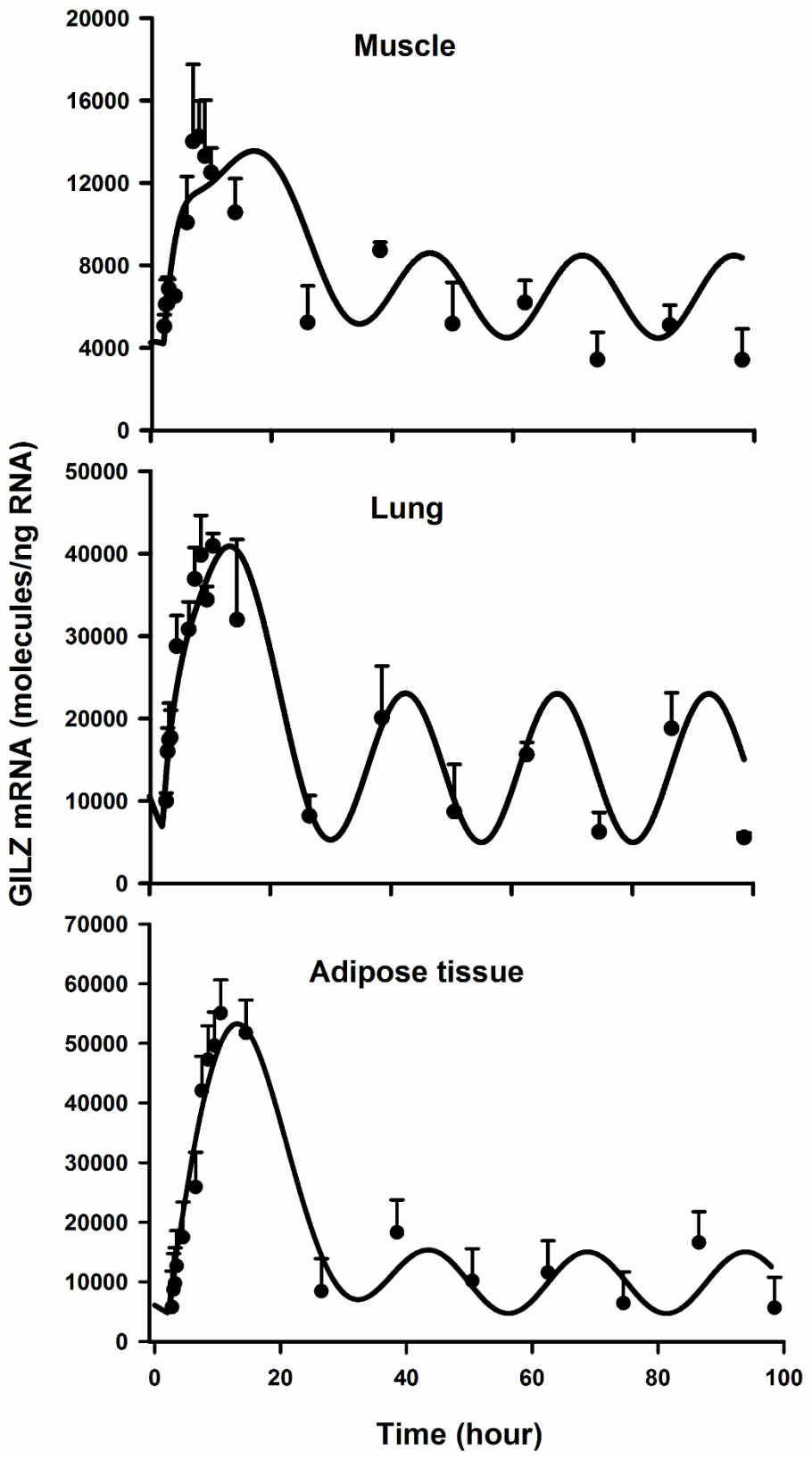

Figure 8

JPET Fast Forward. Published on July 20, 2017 as DOI: 10.1124/jpet.117.242990
This article has not been copyedited and formatted. The final version may differ from this version.

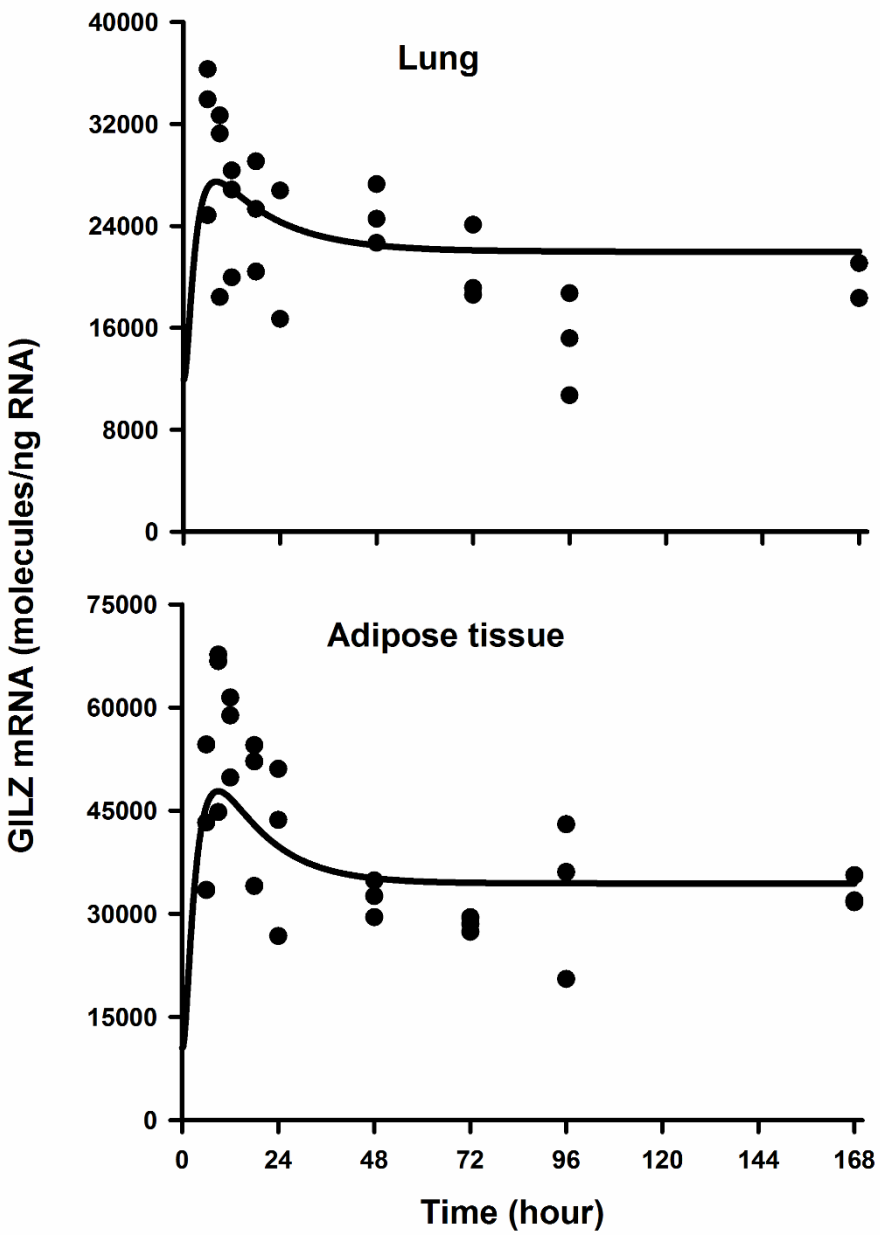

Figure 9

JPET Fast Forward. Published on July 20, 2017 as DOI: 10.1124/jpet.117.242990
This article has not been copyedited and formatted. The final version may differ from this version.

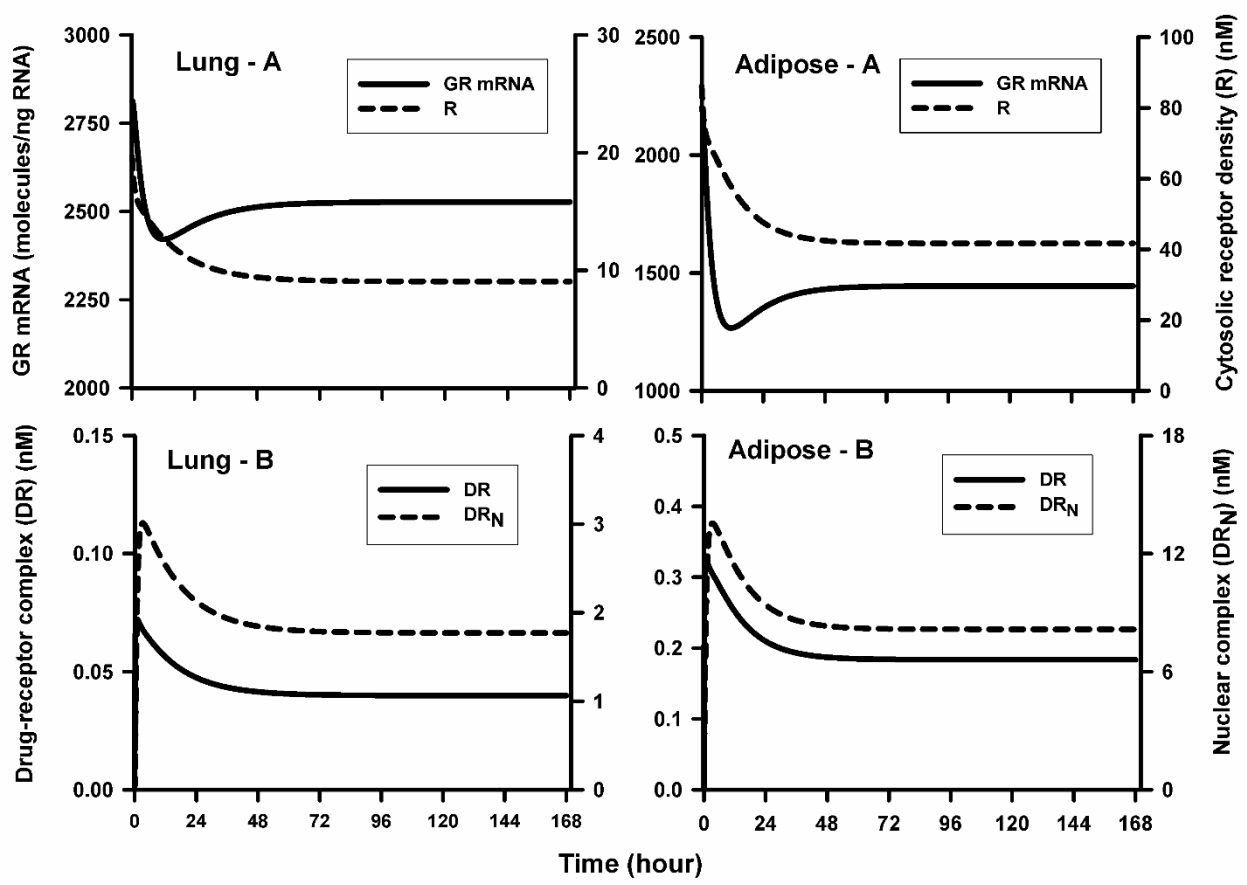

Figure 10